PHYSICAL REVIEW B **94**, 060411(R) (2016)

Large energy product enhancement in perpendicularly coupled MnBi/CoFe magnetic bilayers

T. R. Gao,[1] L. Fang,[1] S. Fackler,[1] S. Maruyama,[1] X. H. Zhang,[1] L. L. Wang,[2] T. Rana,[3,4] P. Manchanda,[3] A. Kashyap,[4,5] K. Janicka,[2] A. L. Wysocki,[2] A. T. N'Diaye,[6] E. Arenholz,[6] J. A. Borchers,[7] B. J. Kirby,[7] B. B. Maranville,[7] K. W. Sun,[2] M. J. Kramer,[2] V. P. Antropov,[2] D. D. Johnson,[2,8] R. Skomski,[3] J. Cui,[9] and I. Takeuchi[1,*]

[1]*Department of Materials Science and Engineering, University of Maryland, College Park, Maryland 20742, USA*
[2]*Division of Materials Science and Engineering, Ames Laboratory, U.S. Department of Energy, Ames, Iowa 50011, USA*
[3]*Department of Physics and Astronomy and Nebraska Center for Materials and Nanoscience, University of Nebraska, Lincoln, Nebraska 68588, USA*
[4]*Department of Physics, The LNM Institute of Information Technology, Jaipur, Rajasthan, India*
[5]*School of Basic Science, Indian Institute of Technology, Mandi, Himachal Pradesh, India*
[6]*Advanced Light Source, Lawrence Berkeley National Laboratory, Berkeley, California 94720, USA*
[7]*NIST Center for Neutron Research, National Institute of Standards and Technology, Gaithersburg, Maryland 20899, USA*
[8]*Department of Materials Science and Engineering, Iowa State University, Ames, Iowa 50011, USA*
[9]*Energy and Environment Directorate, Pacific Northwest National Laboratory, Richland, Washington 99354, USA*

(Received 29 December 2015; revised manuscript received 4 May 2016; published 29 August 2016)

We demonstrate substantial enhancement in the energy product of MnBi-based magnets by forming robust ferromagnetic exchange coupling between a MnBi layer and a thin CoFe layer in a unique perpendicular coupling configuration, which provides increased resistance to magnetization reversal. The measured nominal energy product of 172 kJ/m^3 at room temperature is the largest value experimentally attained for permanent magnets free of expensive raw materials. Our finding shows that exchange-coupled MnBi/CoFe magnets are a viable option for pursuing rare-earth-free magnets with energy products approaching those containing rare-earth elements.

DOI: 10.1103/PhysRevB.94.060411

Finding rare-earth-free alternatives to Nd- and Sm-based permanent magnets has emerged as an urgent technological challenge due to the global economic impact of price instability of rare-earth elements. Among possible candidates, MnBi is one of the few compounds with appreciable intrinsic magnetocrystalline anisotropy. MnBi exhibits coercivity of up to 1.6 T at room temperature [1], and it increases to values as large as 2.6 T at 550 K [1,2]. The high coercivity of MnBi arises from its magnetocrystalline anisotropy, about 1.6 MJ/m^3, and it is very favorable for high-temperature applications, such as in hybrid electric vehicles, but its saturation magnetization is only about $M_s = 640$ kA/m [3,4], limiting the highest achievable energy product to 128 kJ/m^3. The formation of exchange-coupled hard/soft composites is therefore an attractive path to pursue high-energy products in MnBi-based magnets [5,6].

Exchange coupling is ubiquitous in magnetic systems, governing the overall performance of complex magnetic heterostructures and composite materials. Since originally proposed by Kneller and Hawig [7], exchange-coupled nanocomposite permanent magnets have been extensively studied theoretically and experimentally as a means to bolster the energy product of permanent magnets [8–14]. To study the efficacy of exchange coupling in MnBi/soft-magnetic systems, we used density functional theory (DFT) [15,16] to screen candidates and their most favorable interfaces and layer thicknesses [17]. Mn atoms in compounds often favor antiferromagnetic (AFM) sublattices at room temperature [18], and in considering exchange coupling, it is not clear *a priori* whether ferromagnetic (FM) exchange necessary for robust exchange coupling can be established at the interface between MnBi and Co_xFe_{1-x}.

We performed DFT calculations to explore the interfacial energy differences $\Delta\gamma = \gamma(\text{AFM}) - \gamma(\text{FM})$ between antiparallel (AFM) and parallel (FM) magnetic-moment alignments across the interface for MnBi/Co_xFe_{1-x} exchange-coupled layers with different compositions and soft-layer thicknesses (see Fig. 1). We calculated $\Delta\gamma$ to identify the most favorable moment alignments. To rapidly assess the magnetic properties, namely, the energetically favored element (i.e., Co or Fe) at the interface, and the layer thickness that most favors FM alignment for best exchange coupling, we carried out an expedited scan using periodically repeating MnBi/Co_xFe_{1-x} multilayers for trends (see Fig. 1).

To explore trends, we built a multilayer interface as a commensurate stacking of slabs of varying thicknesses along MnBi(0001) and Co_xFe_{1-x}. MnBi films are known to grow textured with the (0001) orientation [19]. Although bulk Co_xFe_{1-x} is a solid solution [bcc (fcc) on the Fe-rich (Co-rich) side], for simplicity and speed, we used bcc(111) multilayers, allowing us to explore pure Co and Fe, as well as alternating Co and Fe layers in an ordered unit cell [Fig. 1(a)] with a magnetic moment of ~1.5 (2.6) μ_B on Co (Fe). Figure 1(b) shows that the Fe moments at the interface tend to align antiparallel to Mn moments, and the cell magnetization is reduced with a thicker Fe layer, while Co at the interface strongly favors the parallel spin alignment with Mn. For a given system, atomic positions and slab dimensions are aligned and relaxed, so $\Delta\gamma$ reflects mostly the different magnetic alignments at a given slab thickness. The trend predicted by Fig. 1(b) is that Co at the interface is more beneficial to the exchange coupling and Co-rich alloys favor FM coupling. We have also performed DFT calculations on the dependence of the coupling behavior

*takeuchi@umd.edu

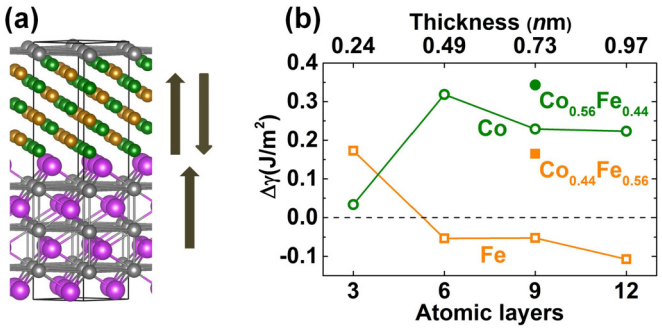

FIG. 1. Density functional theory modeling of MnBi/Co_xFe_{1-x} interface. (a) Unit cell for periodically repeated MnBi(0001)/bcc-CoFe(111), shown with alternating layers of Co (five layers) and Fe (four layers) with Co at the interfaces (corresponding to a $Co_{0.56}Fe_{0.44}$ soft layer). Mn (gray), Bi (purple), Co (green), and Fe (gold) atoms and cell boundaries (lines) are shown. Arrows indicate (anti) parallel alignment of magnetic moments across the interface. (b) Interfacial energy difference $\Delta\gamma$ as a function of atomic layers for multilayer cell (a) having pure bcc Co and Fe, and $Co_{0.56}Fe_{0.44}$ ($Co_{0.44}Fe_{0.56}$) with Co (Fe) at the interface.

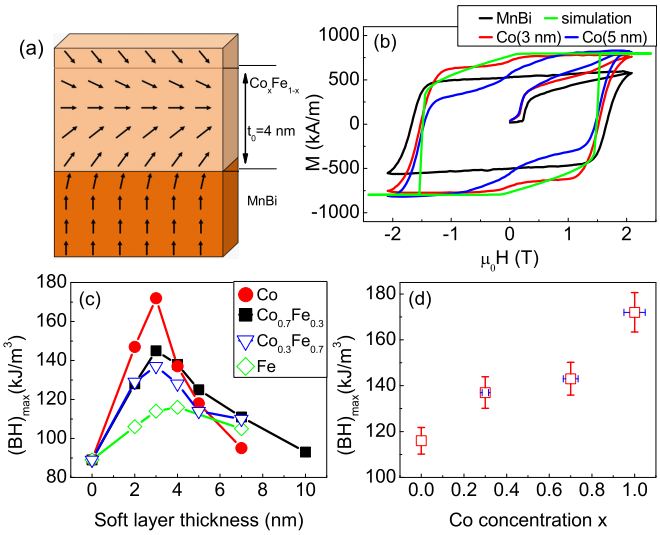

FIG. 2. Large energy product enhancement in perpendicularly coupled MnBi/Co_xFe_{1-x} bilayers: (a) micromagnetic schematic of the bilayer spin structure in a moderately high reverse field. The arrows indicate the spin directions in the MnBi and Co_xFe_{1-x} layers. t_0 is the critical thickness above which the magnetization of the soft layer has a negative contribution to the total magnetization; (b) experimental hysteresis loops of a pure MnBi, MnBi/Co (3 nm), and of MnBi/Co (5 nm) bilayers with the magnetic field perpendicular to the film plane, and simulated hysteresis loop of MnBi/Co (3 nm) bilayer (green line). We note that magnetization values in the experimental curves have been adjusted to take into account a small amount of voids formed in the film (≈5% of the total film volume); (c) $(BH)_{max}$ of MnBi/Co_xFe_{1-x} bilayers for different soft-layer compositions and thicknesses; (d) experimental $(BH)_{max}$ as a function of Co concentration x of Co_xFe_{1-x} for bilayers with 3 nm of soft layer. The uncertainty of 24 kA/m for the saturation magnetization of MnBi film in the text arises from the uncertainty in the thickness measurement.

on the thickness of the soft layer, and the predicted trend is that the strongest FM coupling for bilayers is found for a 2–3 nm Co-rich soft layer [17].

Using this information, we then carried out experiments on thin-film bilayers as a model system consisting of 20 nm MnBi and soft-magnetic Co_xFe_{1-x} of different compositions and thicknesses. To synthesize MnBi, Bi and Mn layers were sequentially deposited on Si(100) substrates at room temperature by a high-vacuum magnetron sputtering system (base pressure 10^{-8} Torr) equipped with four sputtering guns. The room-temperature deposited Bi and Mn layers were post-annealed at 300 °C *in situ* in high vacuum to form MnBi films. The Co_xFe_{1-x} layers with different compositions and thicknesses were deposited on top to establish exchange coupling after the annealed MnBi films are cooled down naturally to room temperature in vacuum. The bilayers were all capped with a 3 nm layer of Pt or SiO_2 to prevent oxidation, and we have checked that the capping does not affect the magnetic properties. The thicknesses of the films were checked using a scanning electron microscope, x-ray reflectometry, and transmission electron microscopy (TEM). Wavelength dispersive x-ray spectroscopy indicates a Mn/Bi atomic concentration ratio of 50:50. X-ray diffraction and TEM are used to determine the crystal structure and the interface structure between the MnBi and substrate. The magnetic properties are characterized by vibrating sample magnetometry (VSM), x-ray magnetic circular dichroism (XMCD), and polarized neutron reflectometry (PNR).

Magnetic properties of MnBi/Co_xFe_{1-x} bilayer films with different thickness and composition combinations of Co_xFe_{1-x} measured with VSM are shown in Fig. 2. MnBi thin films [(0001) oriented] grow with strong columnar texture leading to robust out-of-plane magnetic anisotropy [19]. On the other hand, soft-magnetic thin films Co_xFe_{1-x} deposited on Si possess in-plane anisotropy due to shape anisotropy. We have discovered that perpendicularly exchange-coupled configuration of MnBi/Co_xFe_{1-x} bilayers shown in Fig. 2(a) with Co as the soft layer leads to a significant energy product enhancement. The optimum thickness of the MnBi layer was found to be 20 nm for maximizing the energy product. Figure 2(b) shows typical room-temperature out-of-plane hysteresis loops of a MnBi (20 nm) layer, a MnBi (20 nm)/Co (3 nm) bilayer, and a MnBi (20 nm)/Co (5 nm) bilayer. The pure MnBi film shows strong perpendicular anisotropy with out-of-plane coercivity (H_C) of 1.6 T and saturation magnetization of 600 ± 24 kA/m. By comparison, MnBi (20 nm)/Co (3 nm) and MnBi (20 nm)/Co (5 nm) bilayer films both exhibit reduced coercivity and enhanced remanence, indicating that a perpendicular exchange coupling is established between the MnBi and Co films [20,21].

The initial magnetization of the single MnBi layer is nearly zero in small fields and exhibits a step in fields close to 0.3 T. Such steps normally indicate pinning-controlled magnetization reversal, but the columnar structure of the MnBi layer does not support the underlying lateral motion of domain walls. Our explanation of the initial curve is that the magnetic moment in each column is randomized after thermal demagnetization, meaning that half of the columnar moments point in a downward direction. In a field of about 0.3 T, the initially downward-pointing moments switch upward. In the MnBi/Co bilayers, the Co layer couples to

neighboring columns ferromagnetically and thereby reduces the initial switching field.

We have systematically looked at the major hysteresis loops of bilayers with varying Co layer thicknesses (2–7 nm). While the bilayers with Co thicknesses larger than about 4 nm show marked steps in the hysteresis loops, the step feature is substantially diminished for Co thicknesses of less than 4 nm, indicating that the bilayer films undergo a transition from a rigidly exchange-coupled magnet to exchange-spring behavior as the soft-layer thickness is increased [22].

Let us first consider the spin state at remanence, that is, in zero magnetic field. The magnetocrystalline anisotropy of the MnBi causes the Mn spins to be perpendicular to the film plane, and the robust exchange coupling between the MnBi and Co layers keeps the Co spins in the same direction as long as the Co layer is sufficiently thin. In a reverse field, the spins near the surface switch first, as shown in Fig. 2(a). The green curve in Fig. 2(b) shows the result of micromagnetic simulations for 3 nm Co, which were performed using a Monte Carlo method with the size of the micromagnetic block set to 1 nm.

The most striking feature of the present hard/soft exchange-coupled films is the significant enhancement of the nominal maximum energy product $(BH)_{\max}$. Figure 2(c) shows the energy products for MnBi/Co, MnBi/$Co_{0.7}Fe_{0.3}$, MnBi/$Co_{0.3}Fe_{0.7}$, and MnBi/Fe bilayers with different soft-layer thicknesses [the demagnetization factor of $D = 0.6$ was used for calculating $(BH)_{\max}$]. For all soft-layer compositions Co_xFe_{1-x}, $(BH)_{\max}$ initially increases sharply with the soft layer thickness, reaches a maximum, and eventually decreases. The $(BH)_{\max}$ of pure MnBi films is $89(\pm 6.2)\,\mathrm{kJ/m^3}$, and it increases to $172(\pm 8.6)\,\mathrm{kJ/m^3}$ for 3 nm Co and then gets reduced to $95(\pm 5.7)\,\mathrm{kJ/m^3}$ for 7 nm Co. Composition-wise, for the optimum soft-layer thickness of 3 nm, we found that the energy product monotonically increases with the Co concentration [Fig. 2(d)]. This result is consistent with the DFT prediction of robust ferromagnetic interface exchange for large Co contents x.

Figure 2(a), obtained by analytical calculations, summarizes the spin state during magnetization reversal for soft Co_xFe_{1-x} layers slightly thicker than 4 nm. The soft-layer spins near the surface reverse first and exert a torque that depends on field strength and the soft-layer thickness. With increasing reverse field, the torque increases and eventually causes the hard MnBi layer to reverse at H_c.

Depending on the soft-layer thickness, there are two regimes in the spin reversal behavior. In layers thicker than about 4 nm, the top spins rotate easily, because the finite exchange stiffness in the soft layer, of the order of 10 pJ/m [23], limits the effect of the interface exchange to a few nanometers. This is clearly visible in the experimental blue curve (Co layer: 5 nm) in Fig. 2(b): compared to the red line (Co layer: 3 nm), the remanence is reduced and magnetization rapidly decreases in the second quadrant. For soft-layer thicknesses of less than 4 nm, the top spins are difficult to reverse, and relatively high reverse fields are necessary to rotate them into the film plane. This unique perpendicular coupling configuration has two advantages. First, the soft-layer spins close to the interface with MnBi maintain a large perpendicular magnetization component even in reverse fields, as depicted in Fig. 2(a). Second, since the magnetization of Co_xFe_{1-x} is

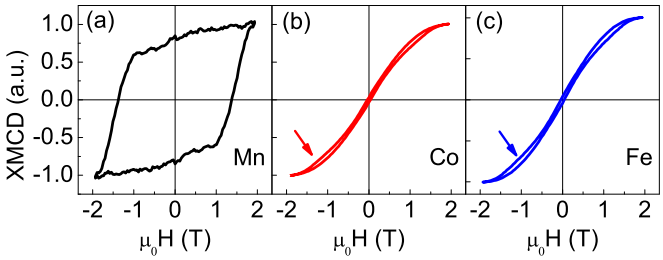

FIG. 3. X-ray magnetic circular dichroism (XMCD): Out-of-plane element-sensitive XMCD hysteresis loops for MnBi (20 nm)/$Co_{0.7}Fe_{0.3}$ (5 nm) Mn (a), Co (b), and Fe (c).

higher than that of MnBi, shape anisotropy favors an in-plane orientation of the magnetization in regions farther away from the hard-soft interface. This preferred magnetization direction has a positive effect in the second quadrant of the hysteresis loop, where the energy product is determined: it stabilizes the magnetization of the soft layer against downward rotation. The result is an enhanced energy product, as displayed in Fig. 2(c). It is also important to note that this mechanism survives in the bulk if one aims at stacking these bilayers in a superlattice-like configuration.

To obtain layer-specific experimental information, we performed XMCD measurements with energy of 165 eV at the Beam Line 4.0.2 at the Advanced Light Source. Figures 3(a)–3(c) show typical element-specific "local" hysteresis loops for Mn, Co, and Fe in bilayers with 5 nm $Co_{0.7}Fe_{0.3}$, where the magnetic field is parallel to the polarized x-ray beam and perpendicular to the sample surface. The hysteresis loop of Mn [Fig. 3(a)] reveals an out-of-plane Mn coercivity of 1.4 T. The out-of-plane coercivities of Co and Fe are much smaller (about 0.2 mT), but the clear broadening of the hysteresis-loop widths at the coercivity of Mn [the arrows in Figs. 3(b) and 3(c)] indicate coupling to the Mn moments. Since XMCD is a surface-sensitive method, it preferentially monitors the spins at the surface. As a consequence, Figs. 3(b) and 3(c) are basically the hysteresis loops for the surface spins in Fig. 2(a). The simulation of the x-ray absorption spectrum and XMCD signal [17] also confirm that the magnetization direction in the $Co_{0.7}Fe_{0.3}$ layer is depth dependent and cants towards the film plane as the distance from the MnBi interface increases.

A very direct verification of the complex MnBi/Co_xFe_{1-x} spin configuration is provided by PNR measurements carried out at Polarized Beam Reflectometer and Multiple Angle Grazing Incidence K (vector) reflectometers at the NIST Center for Neutron Research [24]. In one set of measurements at room temperature, we tracked the field-dependent evolution of the local spin structure in MnBi (29 nm)/$Co_{0.7}Fe_{0.3}$ (4 nm) bilayer with a Pt capping layer of approximately 6 nm. After first saturating the out-of-plane magnetization in a large positive perpendicular field (2000 mT), a negative out-of-plane field was applied, changing from -5 mT to -700 mT. For all measurements the raw data were corrected for instrumental effects such as polarization efficiency (>97%), background, and beam footprint [25]. The magnetization magnitude can be directly calculated from the magnetic scattering length density (SLD) since it is directly proportional. These profiles, which are shown in Fig. 4, thus provide a measure of the depth

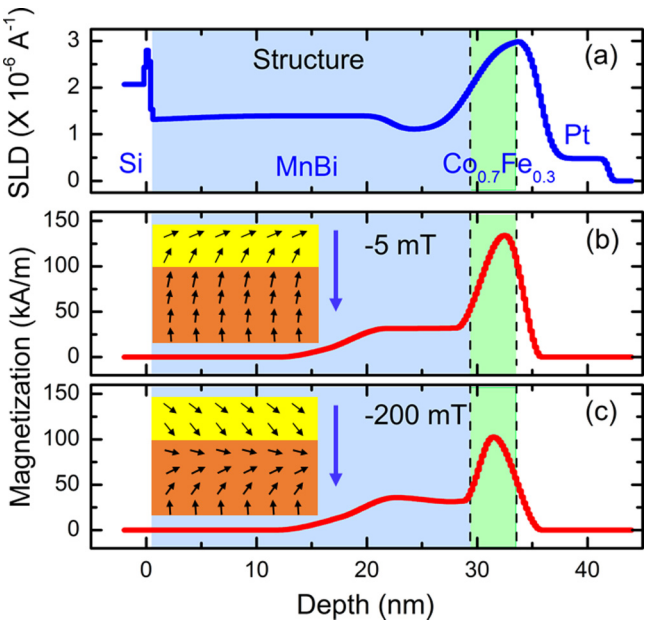

FIG. 4. Reversal mode in MnBi/$Co_{0.7}Fe_{0.3}$ is probed by polarized neutron reflectometry: (a) depth profiles of the structure. $Co_{0.7}Fe_{0.3}$ and MnBi layer regions are indicated by green and light blue, respectively. (b), (c) In-plane component of the magnetization (red lines) obtained from fits to polarized neutron reflectometry measurements where the bilayer was first magnetized in the out-of-plane directions (+2000 mT), and reversed out-of-plane field was applied in the order of −5 mT (b), and −200 mT (c). Yellow and brown denote the $Co_{0.7}Fe_{0.3}$ and MnBi in the OOMMF simulation insets. In (b) and (c), the blue arrows describe the magnetic field direction and the short black arrows depict the corresponding successive evolution of the magnetization profile.

dependence of the nuclear composition, in-plane magnetization magnitude and in-plane magnetization direction, all averaged across the sample plane since the neutron coherence length within this plane is approximately 100 μm.

Figure 4(a) shows the nuclear depth profile obtained from fits to the non-spin-flip data [24]. The structural SLD is equal to the number density of the material times the neutron scattering length characteristic of the material. The depth profiles for the in-plane magnetization obtained from freeform fits [25] to the spin-flip reflectometry data taken in the out-of-plane fields of −5 mT and −200 mT after saturating it in 2000 mT are shown in (b) and (c), respectively. The approximate boundaries between the nominal MnBi, $Co_{0.7}Fe_{0.3}$, and Pt layers are designated on these profiles. The obtained depth profile of magnetization indicates that the in-plane component of the magnetization is mostly isolated within the $Co_{0.7}Fe_{0.3}$ layer in a field of −5 mT following positive saturation. Higher field data are consistent with a gradual spreading of the magnetization into the top region of the MnBi layer as the field begins to increase. The cartoonlike insets in Figs. 4(b) and 4(c), which use magnetization angles from the object oriented micromagnetic framework (OOMMF) simulations, show the spin structures corresponding to the experimental neutron reflectometry data. The numerical cell size used in the OOMMF calculation in Fig. 4 was the same as in the micromagnetic simulations in Fig. 2. For the materials constants, literature data were used [26], as well as a spontaneous magnetization of 576 kA/m and an exchange stiffness of 8 pJ/m for MnBi. The analytical calculations were performed by constructing a nonlinear micromagnetic energy function from approximate magnetization modes and numerically evaluating the function [26–29]. Figure 4 is consistent with the above-outlined micromagnetic spin structure, indicating that our theoretical analyses (DFT, micromagnetism) and experiments (magnetic, XMCD, neutron reflectometry) provide a coherent scientific description of this intriguing system.

In conclusion, we have demonstrated robust ferromagnetic exchange coupling between MnBi and a soft-magnetic layer Co_xFe_{1-x} that results in nominal energy products as large as 172 kJ/m^3 at room temperature. The physical origin of this energy product is a unique perpendicular coupling configuration, which provides increased resistance to magnetization reversal, and involves the micromagnetic stabilization (or "vertical pinning") of the soft-magnetic layer in the second quadrant of the hysteresis loop. While the unique coupling was observed in a bilayer system, the physics is not dependent on the bilayer geometry. Significant strides have been made in synthesis of magnetic particles with aligned magnetization for exchange coupling over the years [30–32]. Given that the present perpendicular coupling effect does not disappear if bilayers are stacked in a superlattice configuration to form three-dimensional magnet structures, it is not unreasonable to imagine synthesis of exchange-coupled anisotropic MnBi/Co magnets in the near future, opening the door for rare-earth-free bulk magnets with high-energy products [33]. While MnBi/Co is not expected to replace the Nd-Fe-B magnets for high-end applications requiring 400 kJ/m^3 [34], there are many midrange applications requiring ∼100–200 kJ/m^3, where new magnets such as MnBi/Co may play a significant role and replace Ba-Sr ferrite, Alnico, and even Sm-Co in the future.

We acknowledge valuable discussions with P. Fischer, J. C. Zhao, D. Arnold, and S. Lofland. Funding for this project was from the Department of Energy ARPA-E REACT (Grant No. 0472-1549). Additional support (computational methods development) at Ames Laboratory was from the Department of Energy, Office of Basic Energy Science, Division of Materials Science and Engineering. Ames Laboratory is operated for the U.S. DOE by Iowa State University under Contract No. DE-AC02-07CH11358.

[1] J. B. Yang, W. B. Yelon, W. J. James, Q. Cai, S. Roy, and N. Ali, J. Appl. Phys. **91**, 7866 (2002).

[2] N. V. R. Rao, A. M. Gabay, and G. C. Hadjipanayis, J. Phys. D: Appl. Phys. **46**, 062001 (2013).

[3] E. Adams, W. M. Hubbard, and A. M. Syeles, J. Appl. Phys. **23**, 1207 (1952).

[4] X. Guo, X. Chen, Z. Altounian, and J. O. Ström-Olsen, Phys. Rev. B **46**, 14578 (1992).

[5] Y. Q. Li, M. Yue, J. H. Zuo, D. T. Zhang, W. Q. Liu, J. X. Zhang, Z. H. Guo, and W. Li, IEEE Trans. Magn. **49**, 3391 (2013).
[6] Y. Q. Li, M. Yue, T. Wang, Q. Wu, D. T. Zhang, and Y. Gao, J. Magn. Magn. Mater. **393**, 484 (2015).
[7] E. F. Kneller and R. Hawig, IEEE Trans. Magn. **27**, 3588 (1991).
[8] R. H. Victora and X. Shen, IEEE Trans. Magn. **41**, 537 (2005).
[9] D. Suess, T. Schrefl, S. Fähler, M. Kirschner, G. Hrkac, F. Dorfbauer, and J. Fidler, Appl. Phys. Lett. **87**, 012504 (2005).
[10] E. E. Fullerton, J. S. Jiang, M. Grimsditch, C. H. Sowers, and S. D. Bader, Phys. Rev. B **58**, 12193 (1998).
[11] R. Skomski and J. M. D. Coey, Phys. Rev. B **48**, 15812 (1993).
[12] B. Balasubramanian, P. Mukherjee, R. Skomski, P. Manchanda, Bhaskar Das, and D. J. Sellmyer, Sci. Rep. **4**, 6265 (2014).
[13] H. Zeng, Jing Li, J. P. Liu, Z. L. Wang, and S. H. Sun, Nature (London) **420**, 395 (2002).
[14] X. Rui, J. E. Shield, Z. Sun, L. Yue, Y. Xu, D. J. Sellmyer, Z. Liu, and D. J. Miller, J. Magn. Magn. Mater. **305**, 76 (2006).
[15] J. P. Perdew, J. A. Chevary, S. H. Vosko, K. A. Jackson, M. R. Pederson, D. J. Singh, and C. Fiolhais, Phys. Rev. B **46**, 6671 (1992).
[16] G. Kresse and J. Hafner, Phys. Rev. B **47**, 558 (1993); **49**, 14251 (1994).
[17] See Supplemental Material at http://link.aps.org/supplemental/10.1103/PhysRevB.94.060411, which includes additional experimental details and results.
[18] M. H. March, J. Mater. Sci. Technol. **17**, 581 (2001).
[19] P. Kharel, P. Thapa, P. Lukashev, R. F. Sabirianov, E. Y. Tsymbal, D. J. Sellmyer, and B. Nadgorny, Phys. Rev. B **83**, 024415 (2011).
[20] J. Sort, A. Popa, B. Rodmacq, and B. Dieny, Phys. Rev. B **70**, 174431 (2004).
[21] A. Bollero, B. Dieny, J. Sort, K. S. Buchanan, S. Landis, and J. Nogués, Appl. Phys. Lett. **92**, 022508 (2008).
[22] N. de Sousa, A. Apolinario, F. Vernay, P. M. S. Monteiro, F. Albertini, F. Casoli, H. Kachkachi, and D. S. Schmool, Phys. Rev. B **82**, 104433 (2010).
[23] R. Skomski, H. Zeng, and D. J. Sellmyer, IEEE Trans. Magn. **37**, 2549 (2001).
[24] C. F. Majkrzak, K. V. O'Donovan, and N. F. Berk, *Neutron Scattering from Magnetic Materials* (Elsevier Science, New York, 2005).
[25] M. R. Fitzsimmons and C. F. Majkrzak, in *Application of Polarized Neutron Reflectometry to Studies of Artificially Structured Magnetic Materials*, Modern Techniques for Characterizing Magnetic Materials (Springer, Berlin, 2005).
[26] R. Skomski, J. Phys.: Condens. Matter **15**, R841 (2003).
[27] W. F. Brown, *Micromagnetics* (Wiley, New York, 1963).
[28] A. Aharoni, *Introduction to the Theory of Ferromagnetism* (Oxford University Press, New York, 1996).
[29] R. Skomski, J. P. Liu, and D. J. Sellmyer, Phys. Rev. B **60**, 7359 (1999).
[30] J. Cui, J. P. Choi, G. Li, E. Polikarpov, J. Darsell, N. Overman, M. Olszta, D. Schreiber, M. Bowden, T. Droubay, M. J. Kramer, N. A. Zarkevich, L. L. Wang, D. D. Johnson, M. Marinescu, I. Takeuchi, Q. Z. Huang, H. Wu, H. Reeve, N. V. Vuong, and J. P. Liu, J. Phys.: Condens. Matter **26**, 064212 (2014).
[31] K. Gandha, K. Elkins, N. Poudyal, X. B. Liu, and J. P. Liu, Sci. Rep. **4**, 5345 (2014).
[32] Y. L. Ma, X. B. Liu, K. Gandha, N. V. Vuong, Y. B. Yang, J. B. Yang, N. Poudyal, J. Cui, and J. P. Liu, J. Appl. Phys. **115**, 17A755 (2014).
[33] R. Skomski, in *Proceedings of Rare Earth and Future Permanent Magnets and Their Applications, 2014* (unpublished), p. 129.
[34] N. M. Dempsey, A. Walther, F. May, D. Givord, K. Khlopkov, and O. Gutfleisch, Appl. Phys. Lett. **90**, 092509 (2007).